LAWRENCE
LIVERMORE
NATIONAL
LABORATORY

LLNL-PROC-636337

Overview of Collisional-Threat-Mitigation Activities at Lawrence Livermore National Laboratory

P. MIller, D. Dearborn, J. Elliott, S. Gibbard, E. Herbold, K. Howley, L. Lomov, R. Managan, A. Miles, M. Owen, J. Rovny, W. Schill, J. Wasem

May 10, 2013

Planetary Defense Conference 2013
Flagstaff, AZ, United States
April 15, 2013 through April 19, 2013

Disclaimer

Planetary Defense Conference 2013
Flagstaff, USA

IAA-PDC2013-04-05

Overview of Asteroid-Threat-Mitigation Activities at Lawrence Livermore National Laboratory

Paul L. Miller[(1)(4)], David S. Dearborn[(1)], James Elliott[(1)], Seran Gibbard[(1)], Eric B. Herbold[(1)], Kirsten Howley[(1)], Ilya Lomov[(1)], Robert Managan[(1)], Aaron Miles[(1)], Michael Owen[(1)], Jared Rovny[(1,2)], William Schill[(1,3)], and Joseph Wasem[(1)]

[(1)]*Lawrence Livermore National Laboratory, PO Box 808, Livermore, CA, 94551*
[(2)]*present address: Yale University, New Haven, CT*
[(3)]*present address: California Polytechnic State University, San Luis Obispo, CA*
[(4)] *corresponding author; email: pmiller@llnl.gov*

Keywords: *asteroid, nuclear, deflection, disruption, porosity, simulation*

Abstract
Nuclear explosives provide a technologically mature and effective means to divert or disrupt asteroids on a collision course with Earth [1]. For scenarios with little warning time before impact, or if the object is large, nuclear explosives are often the *only* option for reducing or eliminating the impact effects. Our investigations at Lawrence Livermore National Laboratory (LLNL) are related to the nuclear approach, including the development of models of impact objects, modeling energy coupling to asteroids, response to the energy deposition, and orbital dispersion. We are evaluating a variety of strategies for a range of realistic scenarios and are assessing current U.S. capabilities. In pursuit of this, we are also conducting verification and validation work, error analysis, optimization studies, and algorithmic and simulation advances. We employ several simulation codes, taking advantage of the strengths of each.

1. Results and Discussion

1.1 Threat scenarios

There is a wide variation among Potentially Hazardous Objects (PHOs) in their size, density, composition, dynamics, and internal structure, among other things. A few asteroids have been studied in detail, yet more have been investigated to a limited degree, and many remain uncharacterized or undiscovered. Without a specific known threat upon which to base our work, we consider a range of cases that span observed behavior and properties. We consider a number of shapes, for example, because the bulk surface topography may affect the amount and distribution of deposited energy. It is well-known that asteroids can be non-spherical. Material composition, especially the surface layer, is important for the depth of energy deposition and for an accurate equation-of-state (EoS) model. The EoS is important to modeling the momentum imparted to the object by blown-off material. Porosity plays a major role in absorbing energy and dampening shocks, and strongly influences the potential for disruption or breakup of the body. The internal structure is central to disruption considerations. "Rubble piles" or fractured rock responds differently to stresses than fully-dense monolithic blocks. The orbit of the asteroid sets how much time is available, how difficult it is to get to the object with a spacecraft, and how material disperses in a disruption event.

1.2 Simulation tools

We are utilizing different simulation capabilities, taking advantage of the strengths of each approach. Codes include Adaptive Smoothed Particle Hydrodynamics (ASPH), ALE rad/hydro, Godunov-based Eulerian with adaptive mesh refinement (AMR), and Lagrangian Finite Element–Discrete Element capabilities. All of these have undergone a range of verification and validation work during their development and previous projects, checking for errors and testing against available analytic, semi-analytic, and empirical results.

The motivation for employing multiple codes is the very wide range of physics involved in modeling the detonation of a nuclear explosive, the subsequent energy production and deposition, the material response to the energy, the evolution of the ablated and shocked material, the response of the object, and the potential disruption and dispersal of the object along its orbit. There is a large range of length and time scales involved, involving behavior successively described by plasma physics, fluid dynamics, solid mechanics, and n-body descriptions. To span these behaviors, we utilize algorithms that are best suited to each regime. A related effort, not detailed here, develops methods for linking and exchanging results between the various codes, in order to track the problem through the different phases.

1.3 Deflection

We are simulating the deflection of asteroids by means of energy deposited by a nuclear explosion. Here, an example uses surface data from Geographos scaled to spherical proportions with a 500-m-equivalent diameter, and a 750 kt nuclear explosion with 150 kt deposited energy (Fig. 1). The graphic combines volume rendering of three quantities: energy density in the ejecta (orange color scale), velocity (RGB color scale), and damage (grey scale).

This simulation was performed relatively early in our project, both as an exploratory case, demonstrating and stretching our ability to model the problem, and as a test-bed for examination of sensitivities. The model incorporated a scaled version of Geographos as a demonstration of our ability to incorporate realistic surface profiles into our simulations. The energy deposition was done as an approximation that included geometric effects and deposition depth, but did not use the full-fidelity deposition at the time because that work was proceeding in parallel. The simulation permitted us to see the effects of porosity and material strength on the subsequent response of the asteroid. It also began our exploration of numerical convergence of the simulations, and introduced the problem of a deflection metric.

The process of energy deposition is the foundation for all deflection and disruption by nuclear explosives. In contrast to a kinetic impactor, there is no net momentum generated in a nuclear explosive deflection. Likewise, there is no "beta" factor, the momentum enhancement factor often discussed in cratering problems, since beta is defined on the basis of the incoming momentum of an impactor [8]. A straightforward deflection metric is the momentum imparted to the main mass of the body. For cases in which the asteroid is neither underdriven (and merely warmed up), nor overdriven (when it may have significant spall off the backside or disrupt in a complicated manner), the deflection is dominated by the surface material that is melted or vaporized. In such a case, the momentum in the vaporized material can be used as a lower bound for the momentum imparted to the object. Assessment of that momentum is closely tied to energy-coupling issues and the material equation of state. The topic is considered in more detail in the paper by Howley, et al., in this proceedings [2].

1.4 Strength, porosity, damage, and fracture modeling

We model objects with strength, and simulate damage and fracture from impulsive deflection events. Porosity has a strong influence on the propagation of shock waves and subsequent damage and fracture behavior resulting from a strong impulsive energy deposition. The resultant shock is damped within the object, affecting its material response significantly. The prospect of spall off the back side of the object — an effect that is detrimental to deflection — is much reduced, and the structure around the cratering side is affected, altering the momentum deposited by solid material thrown off in the cratering process.

In Figure 2, we show simulations of the effect of micro-porosity on the response of a body to a hypervelocity impact. The bulk porosity varies between zero, 20%, and 30%, and the blue-red color scale depicts a damage metric. The strength was also scaled, with strength decreasing as porosity increases, since porous materials are weaker [9]. For the zero-porosity case, spall is observed on the backside of the object, but such a case is not realistic. For more typical 20-30% values of porosity, the spall is absent and the damaged area and cratering response differs. The greater extent of damage at greater porosity is associated with the reduced strength.

1.5 Disruption

Evidence suggests that some asteroids are aggregations of loosely bound fragments, boulders, rocks, and finer particles or regolith. We are modeling such "rubble pile" objects as collections of individual boulders, and are examining the response of the object to the impulse imparted by a nearby nuclear explosion. We employ a Lagrangian Finite-Element code, GEODYN-L, to model the problem. Figure 3 shows two examples of a 500-m object comprised of 2380 individual boulders. The size distribution power law is motivated by reports in the literature [3]. Both objects have the same non-porous density of about 2.38 g/cm^3, the same average porosity of 30%, and the same total volume. The object on the lower left is comprised of boulders with microporosity of 8.6%, with additional gaps (macroporosity) between the boulders explicitly included, contributing an additional 21.4% porosity. The object on the upper right consists of parts that have no gaps between the individual elements, so there is no macroporosity and the parts all have a microporosity of 30%. The asteroid on the lower left can be described as a "gravitational aggregate" and the one on the upper right a "fractured consolidated body." Each is an idealization of a class of asteroid observed and discussed in the literature [4].

Having constructed our model asteroids, we study their response to the impulsive deposition of energy from a nuclear explosion. We consider the deposition of 5.4 kt into the modeled gravitational aggregate. Figure 4 depicts a cross section of the object. The size distribution is shown. Generally the larger pieces are located closer to the center of the asteroid model, and smaller pieces toward the outside. The color cap indicates the location and magnitude of the energy deposition. It drives a shock into the body, putting the boulders into motion. The simulation captures the behavior inside each boulder as well as their interaction with their

neighbors; effectively each boulder is a separate part of an integrated dynamic calculation of the ensemble. Results are shown in Figure 5. Material in the vicinity of the energy deposition vaporizes, melts, or fails, contributing to blowoff. The blowoff imparts momentum to the assemblage of boulders. In the subsequent images in the figures to the right, the blowoff material has been removed for ease of viewing the main object. The orange color scale indicates velocity magnitude.

Asteroids exhibit wide variation in their properties, with rubble piles representing one type. Monolithic objects are another. We examined the disruption behavior of a spherical monolithic iron asteroid subjected to a nuclear explosion. We recognize it is somewhat unrealistic in the sense that there is little evidence for such objects, but it serves as as an extreme case of a strong, unfractured, dense object that is difficult to disrupt.

Figure 6 depicts the response of a 50-m iron sphere of 5% porosity. The image depicts the fragmentation of the object 0.08 seconds after the detonation of a megaton nuclear explosion 15 m from its surface. The various colors depict individual fragments. At the time of the image, the pieces are still undergoing some additional fragmentation. The simulation is conducted with an Adaptive Smooth-Particle Hydrodynamics code named SPHERAL that incorporates models for porosity, strength, damage, and failure. No pieces larger than 3 m are left after the breakup of the object. The cloud of fragments expands so rapidly that even within a day or two, few would impact Earth. For those that did, at sizes of a couple meters or less, the atmosphere provides sufficient protection that they would pose no threat.

1.6 Dispersal

In the case of "rubble pile" type of objects, objects necessitating a very large deflection velocity, or for scenarios in which disruption is the goal, a capability to model post-disruption dispersal is needed. We have developed methods to assess the spread of fragments from an object through subsequent orbits. From this, mass deposition amounts and rates on the Earth may be estimated and plotted.

In the case of the disruption of the gravitational-aggregate object described in the previous section, we continued to follow the development of the detailed dynamics of all the contituative parts beyond the disruptive event. In order to approximate the subsequent behavior, the dissembling pieces were treated with an approximation. The velocity statistics were examined and material with velocities less than escape velocity for the total object mass were assumed to remain bounded and were treated as a single remnant object. We found that about 95% of the mass remained bounded and about 5% was thrown off. We linked the remnant body and the other dissembling pieces to an N-body code with Earth and Sun gravity (no self gravity), and propogated the cloud of pieces forward 1.5 years toward what would otherwise have been an Earth impact. The expanding cloud of fragments is distorted into a long, thin distribution by orbital dynamics. The top image in Fig. 7 shows the cloud as it approaches the Earth-Moon system, and the bottom image displays the distorted cloud after it has passed Earth. Earth is indicated by a blue circle and the Moon by a tan diamond. Neither symbol is to scale.

For this scenario, our modeling showed none of the fragments impacted Earth and the remnant body received sufficient velocity change that it also avoided a collision. This example serves as a demonstration of basic feasibility and behavior of a strong disruptive deflection of a moderately large gravitaitonal aggregate. The details, however, are subject to uncertainties of the intial composition of the object, accuracies of the models, and details of the fragmentation process. Additional information would help some of these issues. A survey mission is always desirable, when possible, before a mitigation mission. Even with near-perfect information on the initial object, however, there are some stochastic effects of the fragmentation and dispersal process. Ensembles of calculations could be used to provide a statistical description — of how many fragments are produced, their locations, and trajectories, for example — moving beyond a single deterministic realization.

Another paper by our group describes a new analytic description of the orbital change imparted to an asteroid by an impulsive deflection [5]. We use that framework to explore the propagation of error in deflection velocity to the final Earth-miss distance in order to quantify necessary accuracy in modeling deflection scenarios. Errors arise from a number of sources, and it is important to be able to quantify the consequene of errors when considering the adequacy of a deflection approach.

1.7 Validation

The algorithms and codes used in this work have undergoine a range of validation and verification in their development, both as part of previous work and during this project. One example is validation of fracture and failure behavior, as shown in Fig. 8. The experimental image shows the failure and fracture of an explosively driven metal pipe [6]. The simulation of this high-strain-rate behavior was conducted with our ASPH code SPHERAL. Since fracture depends on details of the microstructure of the material, the comparison is in a statistical sense, for quantities such as the time and location of the onset of crack formation, the crack growth

rates, and the number density of cracks. The results show that the modeling is able to capture many of these aspects of the experiment. We continue to refine the models to further improve their results.

In addition to such validation work consisting of focused tests of particular sub-models, we addresed a large-scale validation problem that serves to integrate many of the related aspects of nuclear deflection and disruption. We simulated a hypervelocity impact upon Mars' moon Phobos, and the resultant formation of the large Stickney crater. The problem is challenging, has been addressed previously in the literature [7], is of interest to the community, and involves many of the aspects of a nuclear deflection or disruption of an asteroid. One drawback is that there is lack of detailed knowledge of the impactor and the internal structure of Phobos, but there are some constraints on the scenarios and good imagery of the topology of the resultant Stickney crater.

Our Phobos-Stickney modeling builds upon previous work [7]. The energy released in the impact event is estimated at approximately 100 Megatons. The crater has a diameter of about 9 km. We used the SPHERAL code to model the interaction of a high-speed impactor with Phobos. The problem evolves on hydrodynamic timescales for the impact, damage, and failure, capturing the initial response of the moon. The formation of the crater takes much longer, and was not practical using a simulation that resolves hydrodynamic timescales. While we plan to develop a means to link the early-time simulation to a late-time n-body simulation with gravity, permitting us to continue the problem through the full crater formation and fall-back of material, we employed an approximation for now. After the dynamics of the crater formation was well underway, we post-processed the simulation and identified material that had sufficient velocity to escape the top of the crater, then removed that material from the visualization of Phobos as an estimate of how the crater would appear. The comparison is shown in Fig. 9.

2. Conclusions

We have described and discussed our work on deflection and disruption of asteroids by means of nuclear explosives. We have approached the problem using a range of codes and methods that address the different regimes of behavior. We have modeled the integrated problem of the deflection of an asteroid by a nuclear explosion and used it as a basis for more detailed studies of porosity, material strength, and simulation convergence. We have developed techniques to model gravitational aggregates, fractured consolidated bodies, and porous monolithic objects, of various compositions. Examples of the disruption, dispersal, and subsequent orbital dynamics have been simulated in order to determine what, if any, of the material would strike Earth. We engage in a continuing process of validation and verification of our codes and models, testing and examining key physics as well as integrated problems, with the goal of developing a comprehensive modeling capability of the deflection and disruption of Earth-threatening objects.

3. Acknowledgements

This work was funded by the Laboratory Directed Research and Development Program at LLNL under project tracking code 12-ERD-005, and was performed under the auspices of the U.S. Department of Energy by Lawrence Livermore National Laboratory under Contract DE-AC52-07NA27344.

4. References

[1] Defending Planet Earth: Near-Earth Object Surveys and Hazard Mitigation Strategies, Final Report, Committee to Review Near-Earth Object Surveys and Hazard Mitigation Strategies, National Research Council, The National Academies Press, January 2010.
[2] Holsapple, K.A., and Housen, K.R., "Momentum Transfer in Asteroid Impacts. I. Theory and Scaling," Icarus **221**, 875-887 (2012).
[3] Howley, K., et al., this proceedings (2013).
[4] O. Vorobiev, "Generic strength model for dry jointed rock masses", International Journal of Plasticity, **24**, 2221-2247 (2008).
[5] See, for example, Saito J., et. al., Science, **312**, 1341 (2006); Abe, S., et al, "Mass and Local Topography Measurements of Itokawa by Hayabusa", Science **312**, 1344 (2006); and Veverka, J., et al, "NEAR at Eros: Imaging and Spectral Results", Science **289**, 2088 (2000).
[6] Asphaug E., Ostro S.J., Hudson R.S., Scheeres D.J., Benz W., Nature, **393**, 437 (1998).
[7] Wasem, J., et al., this proceedings (2013).
[8] Vogler,, T.J., et al., "Fragmentation of Materials in Expanding Tube Experiments," International Journal of Impact Engineering, **29**, 735-746 (2003).
[9] Asphaug, E., and Melosh, H.J., "The Stickney Impact of Phobos – A Dynamic Model," Icarus **101**, 144-164 (1993).

5. Figure Captions

Fig. 1: A rendering of a scaled-Geographos model with a 500-m-equivalent diameter, subjected to a 750 kt nuclear explosion with 150 kt deposited energy. The graphic combines volume rendering of three quantities: energy density in the ejecta (orange color scale), velocity (RGB color scale), and damage (grey scale).

Fig. 2: Simulation of a hypervelocity impact on an object with microporosity. Color scale represents a damage metric, with blue undamaged and red completely damaged. Microporosity varies between 0, 20%, and 30%.

Fig. 3: Two examples of a 500-m object comprised of 2380 individual boulders. Both have the same density of about 2.38 g/cm^3 and the same total volume, but different amounts of micro- and macroporosity. See text for details.

Fig. 4: Depiction of a cross section of a modeled 500-m gravitational aggregate. The size distribution of the constitutive pieces is shown. The color cap indicates the location and magnitude of the 5.4 kt energy deposition.

Fig. 5: Two images of the response of the object shown in Fig. 4, 1.0 s (top) and 16.27 s (bottom) after detonation. The blowoff material has been removed for ease of viewing the main object. The orange color scale indicates velocity magnitude.

Fig. 6: Fragmentation of a 50-m iron sphere of 5% porosity, 0.08 seconds after a nearby megaton explosion. Colors represent individual fragments (or fragment sources for finer pieces).

Fig. 7: Interaction of a cloud of disrupted fragments before (top) and after (bottom) its interaction with the Earth-Moon system. Earth depicted by circle, Moon by diamond symbol (not to scale).

Fig. 8: Comparison of data [6] and simulation of the dynamic failure of an explosively driven metal pipe.

Fig. 9: Comparison of Phobos image (left) taken by Viking 1, with the Stickney crater to the right side of the moon, with the result from our simulation (right).

6. Figures

Fig. 1:

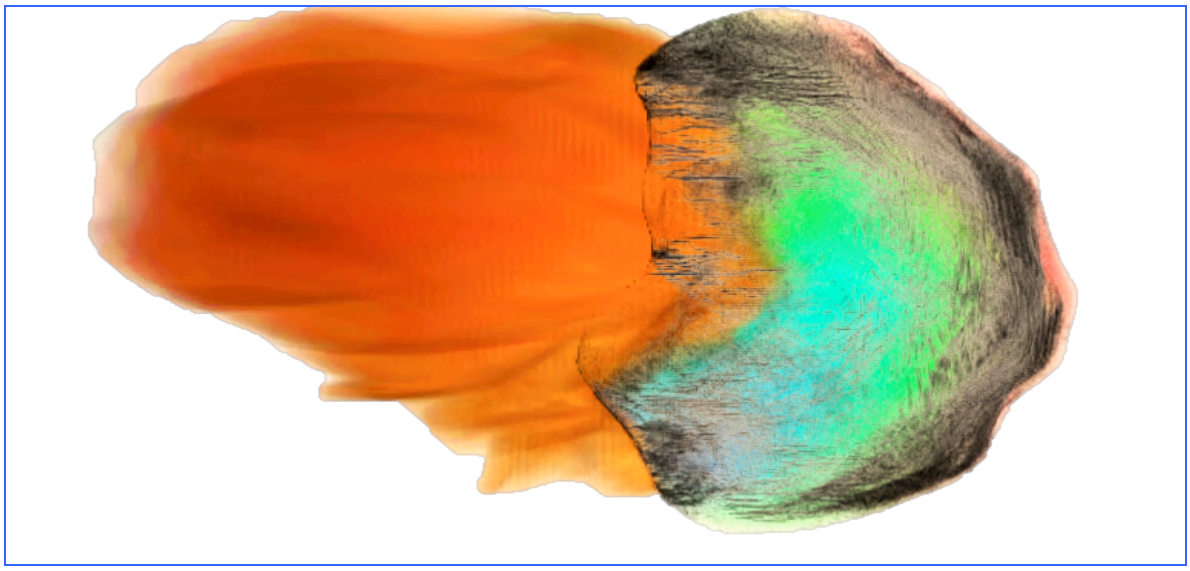

Fig. 2:

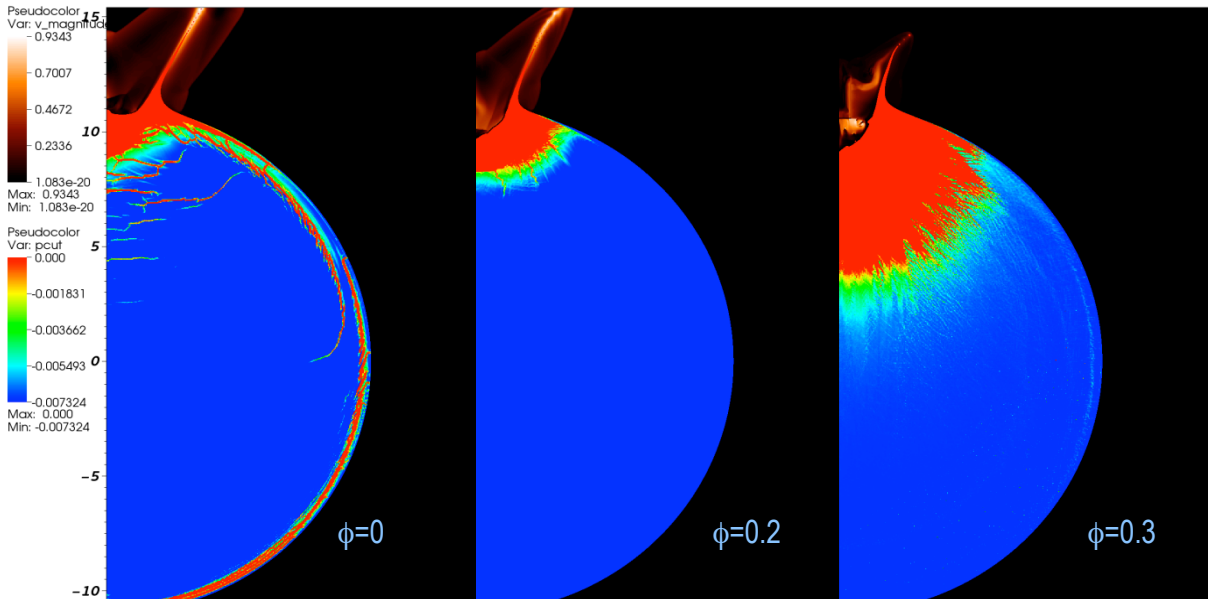
Pseudocolor
Var: v_magnitude
0.9343
0.7007
0.4672
0.2336
1.083e-20
Max: 0.9343
Min: 1.083e-20
Pseudocolor
Var: pcut
0.000
-0.001831
-0.003662
-0.005493
-0.007324
Max: 0.000
Min: -0.007324
15
10
5
0
−5
−10
ϕ=0
ϕ=0.2
ϕ=0.3

Fig. 3:

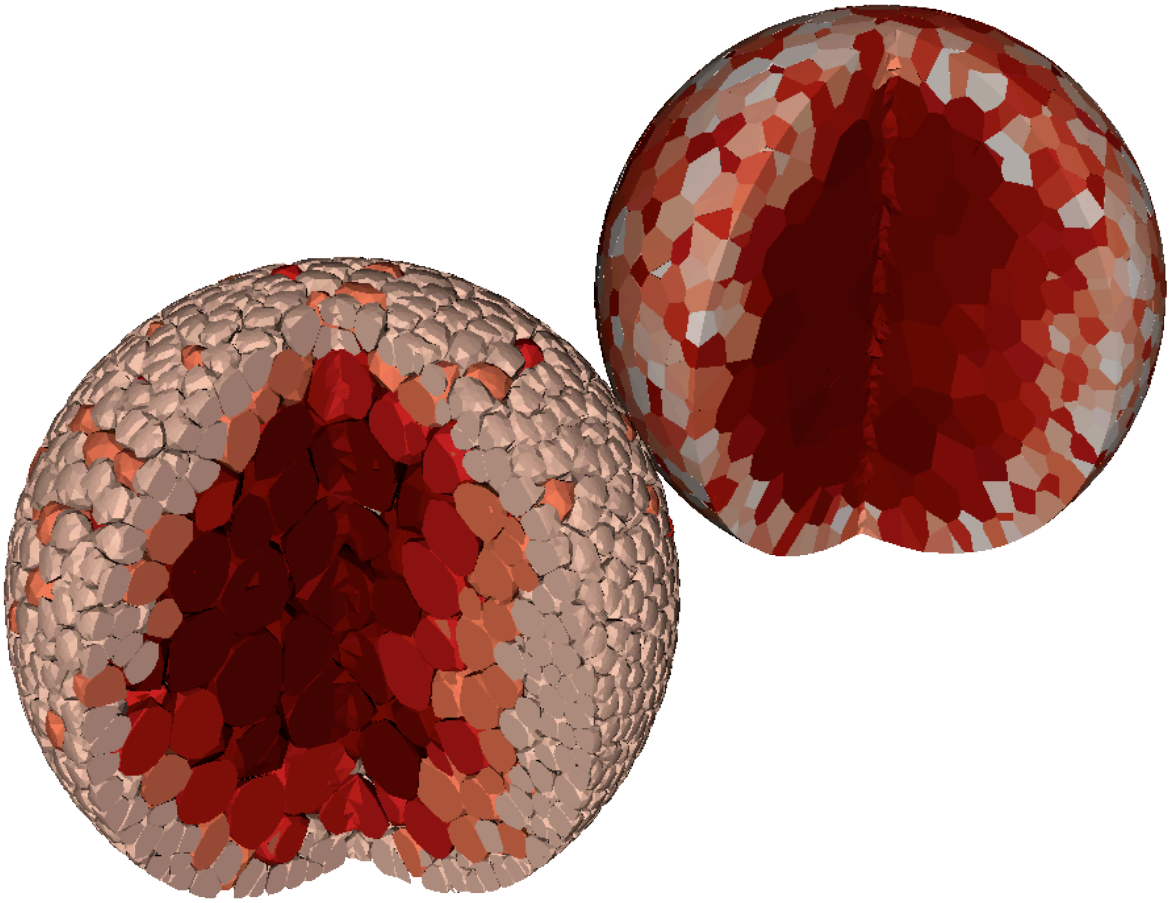

Fig. 4:

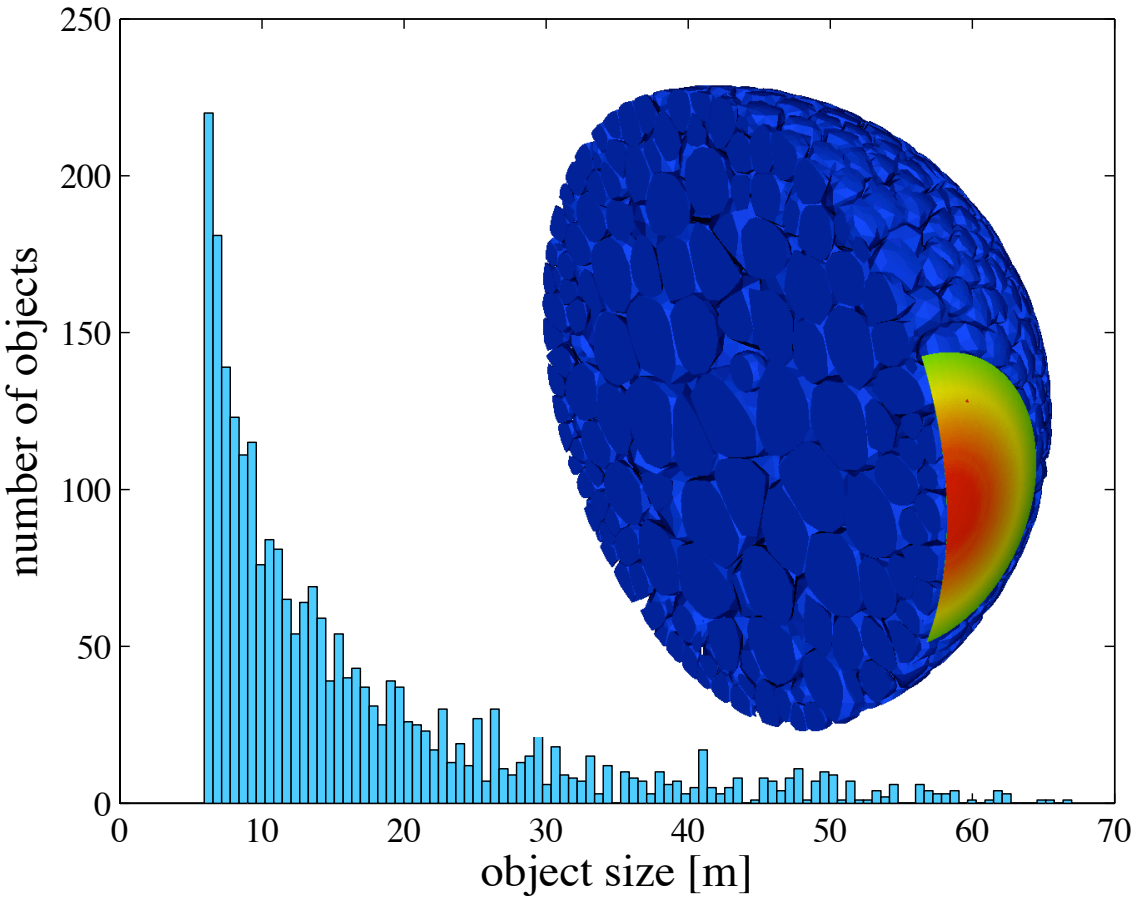
250
200
150
100
50
0
number of objects
0
10
20
30
40
50
60
70
object size [m]

Fig. 5:

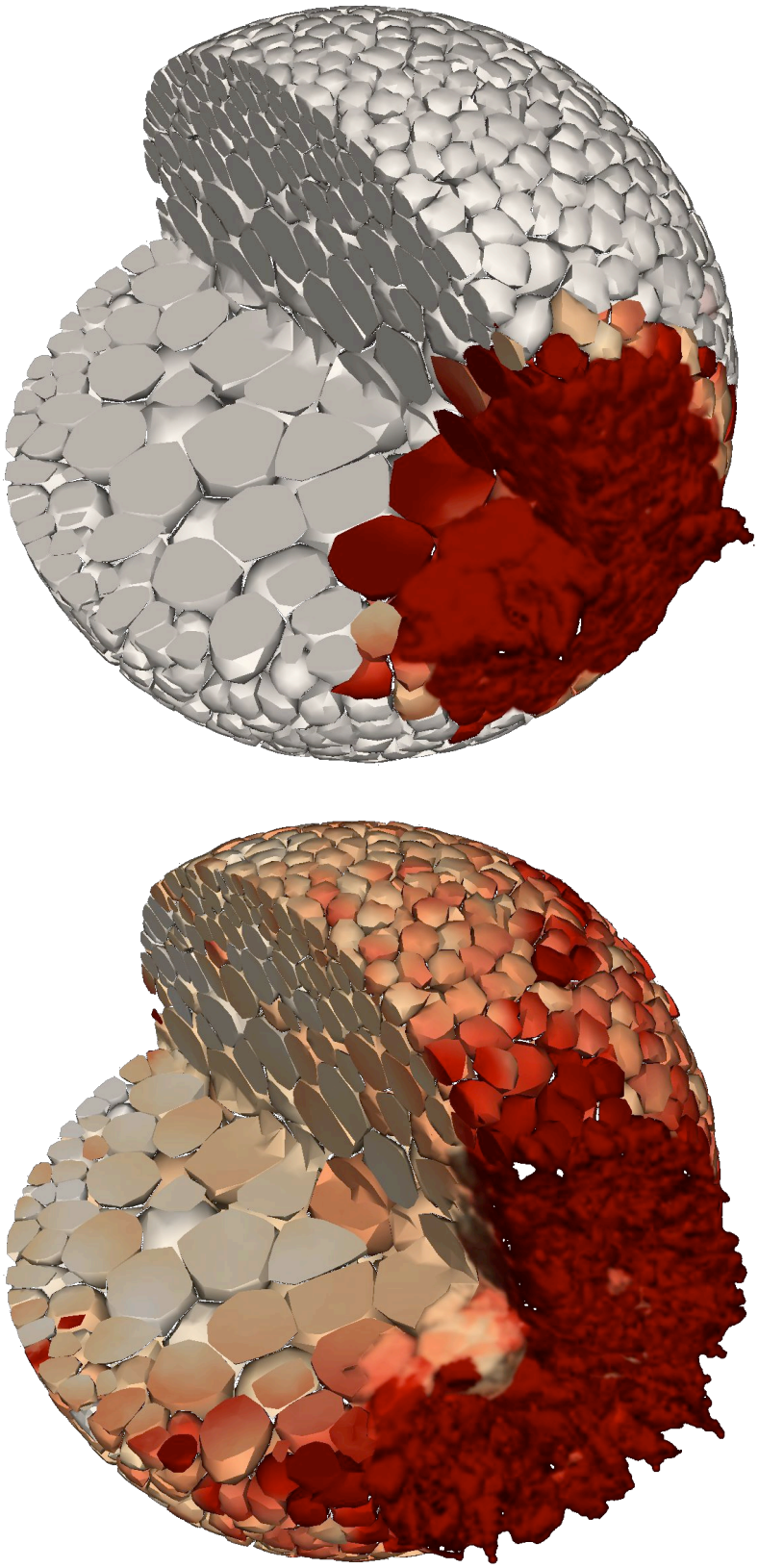

Fig. 6:

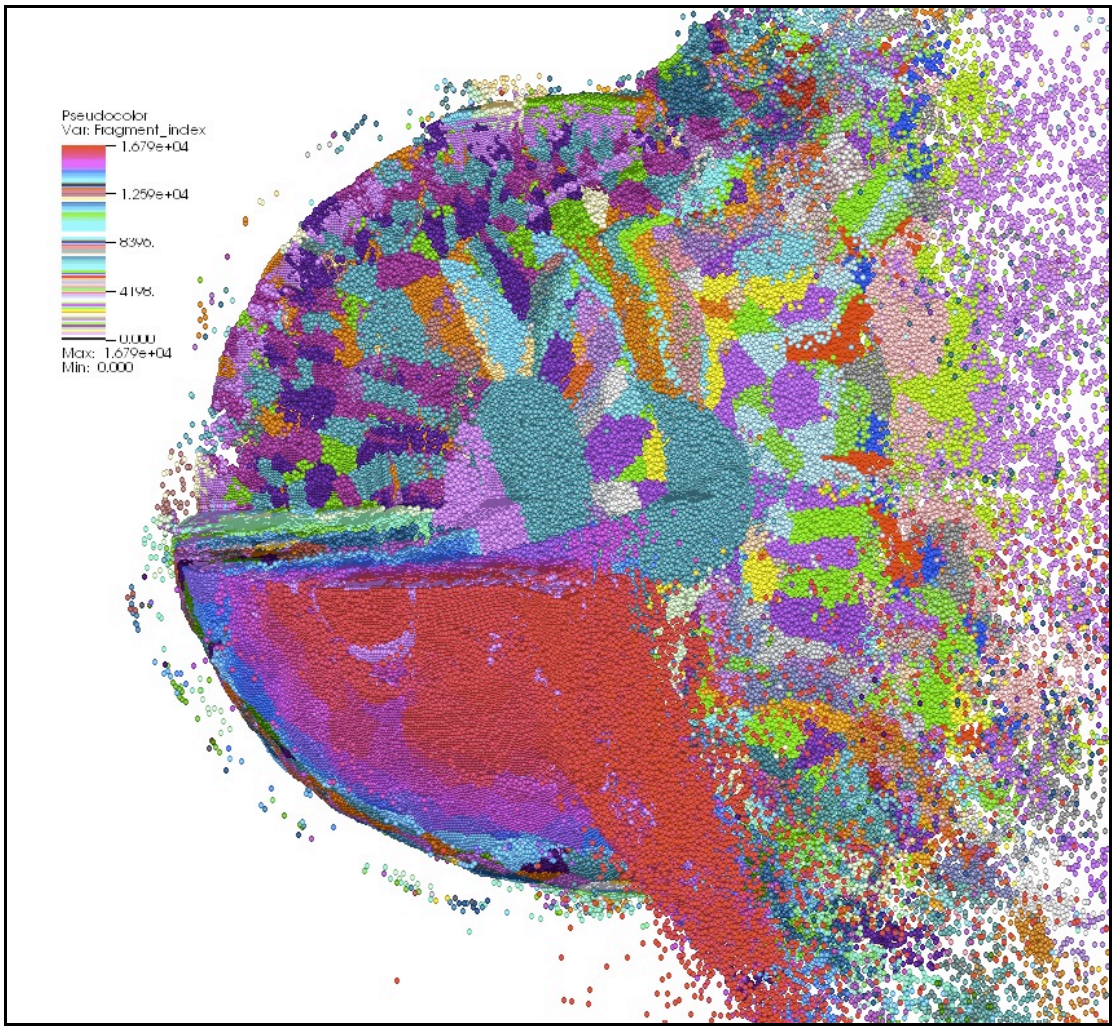
Pseudocolor
Var: Fragment_index
1.679e+04
1.259e+04
8396.
4198.
0.000
Max: 1.679e+04
Min: 0.000

Fig. 7:

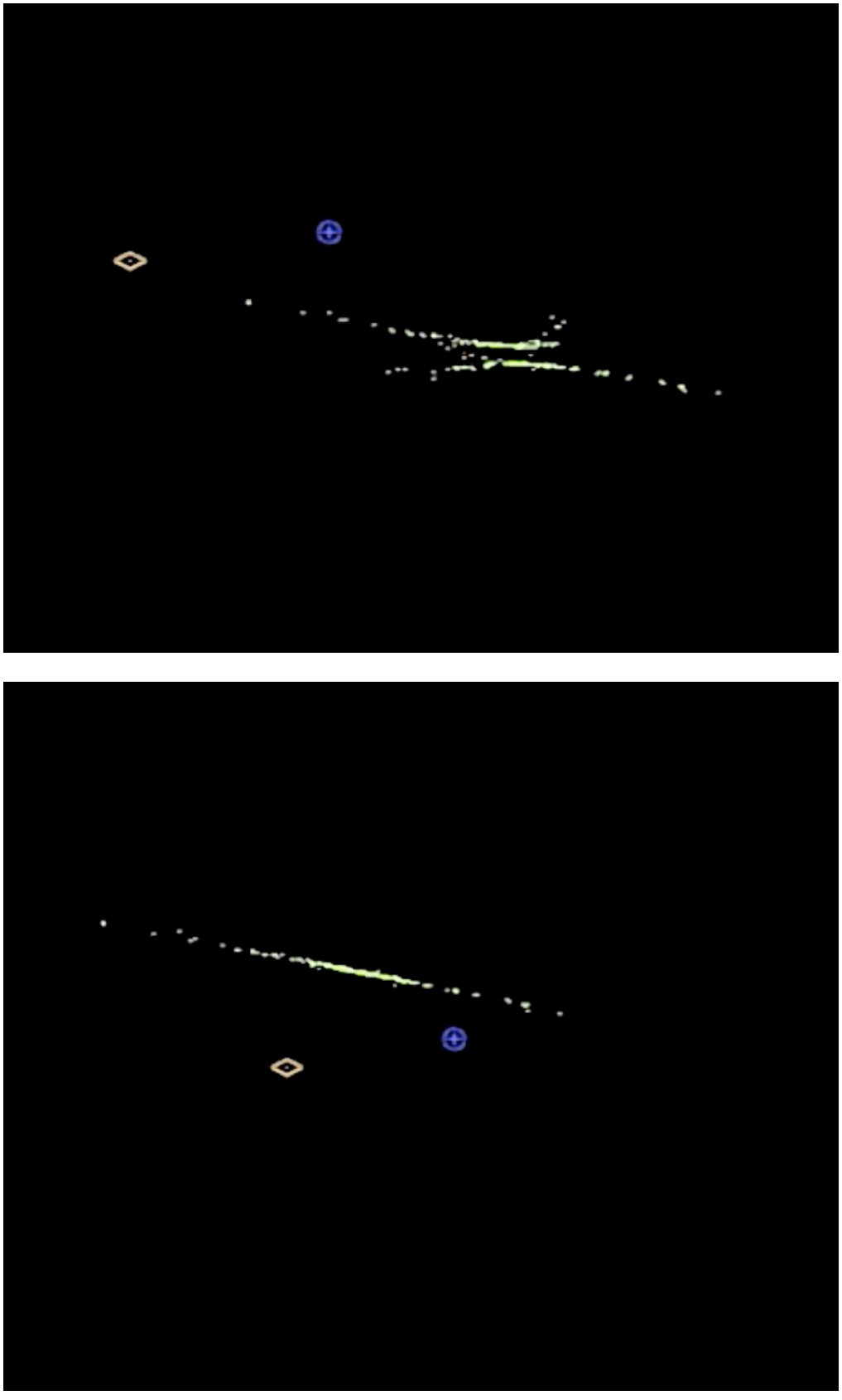

Fig. 8:

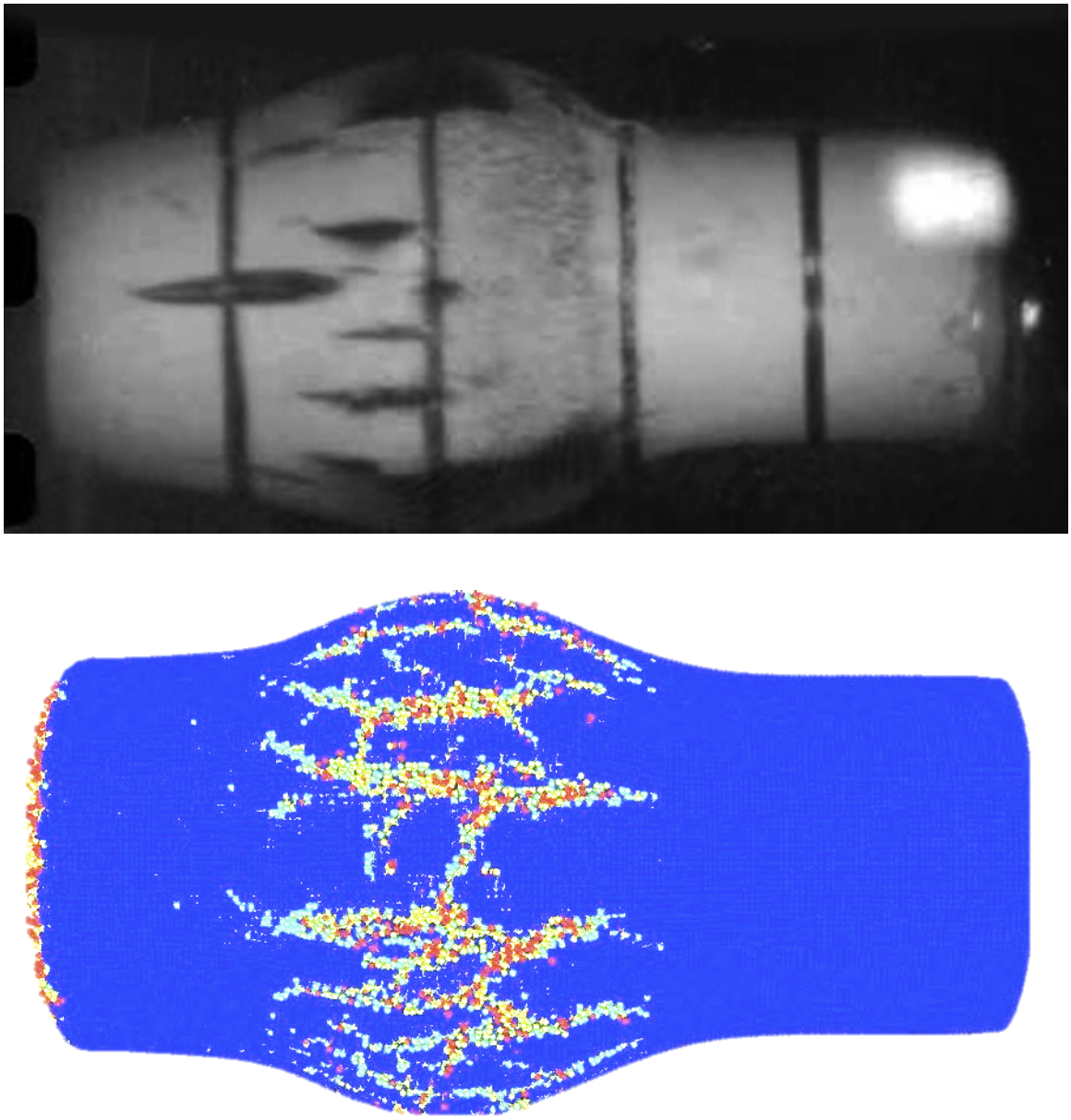

Fig. 9: